A High-Performance 650-GHz Sideband-Separating Mixer—Design and Results

Ronald Hesper, Andrey Khudchenko, Andrey M. Baryshev, Jan Barkhof, and Fausto Patricio Mena

***Abstract*—We presented the design and experimental results of a new sideband-separating (2SB) mixer for 600–720 GHz (ALMA Band 9). Although designed following the classical quadrature hybrid architecture, the emphasis of the optimization was this time not placed on ultimate phase and amplitude balance in the hybrid, but on the reduction and active suppression of reflections and standing waves. It turns out that, once the phase and the amplitude are sufficiently balanced, the image rejection ratio (IRR) starts being dominated by unbalanced parasitic reflections in the signal path, and further perfection of the hybrid's balance is not the way toward higher IRR. Four operational waveguide blocks were produced. IRRs above 15 dB over the entire band were obtained, depending critically on mixer matching. The noise temperature was not more than 20–30 K above the value expected from the individual mixer devices. With the RF circuits optimized thus, the performance becomes limited by the IF system, where similar interference and standing wave problems seem to occur. These are exacerbated when, for compactness (i.e., in arrays), cryogenic isolators between the mixers and amplifiers are omitted. We show that, because of the high performance of the mixers, an IRR of 10 dB can still be obtained without isolators. When, on the other hand, highly matched amplifiers are used, we expect that the full image rejection performance can be achieved even in array receivers. These 2SB mixers are intended for the future 2SB receivers on the APEX (Chile) and LLAMA (Argentina) observatories and for deployment in any other observatory that would benefit from sideband separation in the 600–720-GHz band.**

***Index Terms*—ALMA observatory, image rejection ratio (IRR), sideband-separating (2SB) mixers, submillimeter wave technology, terahertz receivers.**

I. Introduction

A NEW waveguide structure for a 600–720-GHz (ALMA Band 9) sideband-separating (2SB) mixer was recently presented [1]. It was designed mostly from scratch, based on all our findings with the previous generation modular Band 9 2SB mixer [2], [3], that contained the same waveguide structure as the first monolithic demonstrator [4].

At the time of publication of [1], only very preliminary results were available. In this paper, we briefly resume the drivers of the new design, augmented with new insights, and subsequently show measurement data from the extensive testing campaign that was carried out over the last year.

II. Top-Level Design Considerations

Like its predecessors, the waveguide structure is based on the classical quadrature hybrid architecture, micromachined together with local oscillator (LO) couplers and an in-phase LO splitter into a modular waveguide split block [5]. The RF feedhorn and mixer back pieces are separate components and easily exchanged, which makes for very convenient double-sideband (DSB) characterization of the individual mixer devices for matching purposes. The mixer devices are the same superconductor–insulator–superconductor (SIS) devices used in the current ALMA Band 9 receivers.

Although the original structure fulfilled the original ALMA specifications with respect to noise temperature and image rejection, the noise temperature was significantly degraded with respect to the levels obtained by the actual deployed DSB ALMA Band 9 mixers [6]. Interestingly, a marked anticorrelation was observed between the noise temperature and the image rejection ratio (IRR) when mixer blocks of different materials and surface finish were tested [3], which led to the insights on which the new design is based.

A. Waveguide Losses

As can be expected, the loss in the waveguides, responsible for the increase in noise temperature, has two main contributions: the material properties of the walls and the geometry of the waveguide. As it turns out, these contributions were of the same order of magnitude, and therefore, both had to be addressed for optimal results.

A marked increase in loss was observed when comparing gold-plated waveguides to bare copper or copper–tellurium ones. From comparisons between the noise temperatures measured in single-ended configuration and in combination with the hybrid blocks (where each signal run is about 12 mm in length), we estimate a loss in the latter of 3.2 dB for the gold-plated blocks and 1.2 dB in the case of bare copper–tellurium. These losses are about twice as high (in dB/m) as expected from the differences in conductivity using the classical skin effect model [7].

Manuscript received July 14, 2017; accepted September 17, 2017. Date of publication October 23, 2017; date of current version November 8, 2017. This work was supported in part by the Netherlands Research School for Astronomy (NOVA) under a NOVA-IV ALMA R&D grant, in part by the AETHER program of RadioNet under FP7, and in part by the Comisión Nacional de Investigación Científica y Tecnológica under fund CATA-Basal PFB06. *(Corresponding author: Ronald Hesper.)*

R. Hesper, A. Khudchenko, A. M. Baryshev, and J. Barkhof are with the Kapteyn Astronomical Institute, University of Groningen, 9712 CP Groningen, The Netherlands (e-mail: R.Hesper@astro.rug.nl; A.Khudchenko@sron.ml; A.M.Baryshev@astro.rug.nl; J.Barkhof@sron.nl).

F. P. Mena is with the Department of Electrical Engineering, Universidad de Chile, 8320000 Santiago, Chile (e-mail: fpmena@u.uchile.cl).

Color versions of one or more of the figures in this paper are available online at http://ieeexplore.ieee.org.

Digital Object Identifier 10.1109/TTHZ.2017.2758270

Very likely, surface roughness and stresses in the wall material will play an increasing role as the frequencies increase, at some point dominating the (bulk) material properties. In addition, at the frequencies under consideration here, the skin effect model starts to break down as the calculated skin depth approaches the electron mean free path in the metal (which can be considerably longer in the cryogenic case than at room temperature), and we enter the so-called anomalous skin-effect regime [8], [9]. Although we did not perform extensive theoretical calculations or modeling of these effects, we believe that together they can account for the unexpectedly high losses in gold-plated surfaces as compared to bare copper.

Irrespective of the resistive mechanism, the geometry of the waveguide plays a decisive role in the loss, as generally known. Basic model calculations confirm that the 310 $\times$ 145 μm waveguides used in the original structure have a loss per unit length almost twice as high as ones of 400 $\times$ 200 μm, which is close to the maximum possible size for this frequency range while keeping them single-moded. Because of the modular nature of the block, necessitating longer waveguide runs, this hit us harder than in the monolithic case for which the structure was initially designed.

The bottom line is that with frequencies approaching or exceeding the teraherz, loss problems may be reduced by choosing the waveguide dimensions as large as possible compatible with single-moded operation and manufacturing them out of a low-loss material like pure or at most weakly alloyed copper.

B. Unbalanced Interference Effects

As mentioned above, in the previous development phase, we noticed a clear anticorrelation between noise temperature and IRR [3]. Initially, we simply attributed this to various standing waves [1], which become more and more suppressed when the waveguide losses (and hence the noise temperature) go up. Recently, more detailed studies [7] revealed that the main offending mechanisms are actually not standing waves in the strict sense, but rather asymmetrical reflection paths inherent in the used 2SB architecture. There are, of course, many potential reflections off the mixers and waveguide components that could (and probably do) cause various degrees of standing waves, but most of them are symmetrical with respect to the two branches of the signal path and, in the first order, do not influence the amplitude and phase balance and, therefore, do not impact the IRR. A good example is the LO path, where high-level signals are present. A significant part of the LO power will reflect from either mixer, back through the LO coupler, and, because of the hybrid's finite isolation, to the other mixer. This path, however, is fully symmetric between the two sides of the structure and will not contribute to the degradation of the IRR (provided that the structure is machined symmetrically and the mixer reflections are equal). Note that, although the IRR is not impaired by symmetrical reflections, they may still cause other grief like standing waves that could result in unacceptable passband ripple, for instance. For this reason, minimizing *any* reflection is worthwhile, but, usually, there are tradeoffs, and the stress in our case is on optimizing the image rejection.

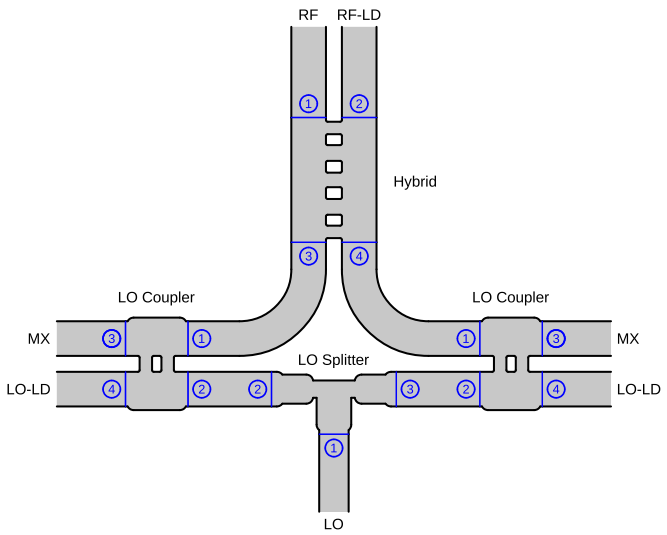

Fig. 1. Central part of the waveguide structure. Port labels as follows. RF: input from feedhorn, RF-LD: RF load, LO: LO input, LO-LD: LO load, MX: mixer. The encircled numbers denote the port numbers of the individual components, as referred to in the text.

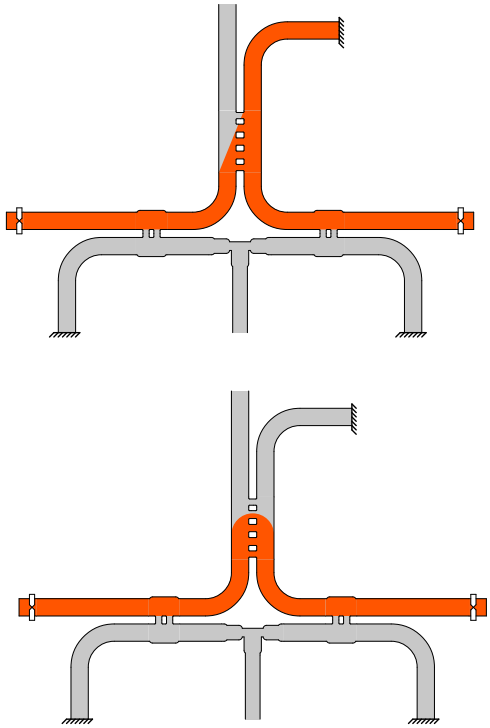

Fig. 2. Two reflection paths that cause most of the deterioration of the image rejection, when the contributions of the amplitude and phase balance are accounted for. See main text for detailed explanation.

Fig. 1 shows the core of the waveguide structure. The component port numbers used in the following discussion are marked in circles.

We identified two major ways that unbalanced interferences can occur, as illustrated in Fig. 2. The first one is when the reflections from each SIS device pass back through the hybrid to interfere constructively at RF load port 2 (and, incidentally, destructively at RF input port 1), after which any reflection from

the load is redistributed equally over the mixers through ports 3 and 4. Careful counting of the cumulative 90° phase shifts in the hybrid reveals that, whenever due to the overall phase rotation in the system, the direct and reflected signals arrive in phase in one mixer, they are in precisely in antiphase in the other. More generally, the "error" signal arriving at either mixer, when considered as a vector in phase space, rotates with a more or less constant magnitude as a function of frequency, but is always in quadrature with the one arriving at the other mixer, which together with the additional 90° shift of the direct signal to that other mixer means they always end up in relative antiphase. Because this mechanism causes opposite error vectors in the two mixers, they have a maximum detrimental effect on the IRR, which is determined by the magnitude of the vector difference between the error signals.

The second path is from either SIS device to the other by taking a "U-turn" through the hybrid (corresponding to S_{43} and S_{34} parameters, usually called the hybrid's isolation). Although the detailed accounting of $\pm 90°$ phase shifts is different, the total effect is precisely the same. The rotation rate of this error signal is of course different due to the different path lengths involved.

The periods of these two mechanisms, determined by the total length of the involved waveguide runs, correspond quite closely to the experimentally determined pumping balance of the mixers [7]. Interestingly, because of the above-mentioned vector nature of the interference, neither of these mechanisms would result in a periodicity of the IRR, just in an overall deterioration. It is the fact that both are present, with different periods, that an interference pattern appears in the image rejection ratio as function of frequency.

Together, these paths share three equally important contributions impacting the IRR: the input reflection of the SIS devices, the input reflection of the RF waveguide load, and the isolation of the hybrid. If any two out of these three can be made arbitrarily small, the IRR degradation caused by unbalanced interference effects should vanish. The input reflection of the SIS devices is about -8 to -10 dB in our case, based on the amplitude of the observed pumping imbalance [7], which is, in turn, consistent with what is known about the SIS design. This is not something that can easily be improved without a total SIS redesign. That leaves only the waveguide load terminating hybrid port 2 and the isolation (S_{43} and permutations) of the hybrid itself to improve. The former was addressed, instead of developing a completely new load, by placing a distributed attenuator in front of the existing load, in the form of a long waveguide run covered with high-resistivity material (sputtered titanium in this case). We estimate that this reduces the load reflection by about 8 dB. As for the latter improvement, since the new hybrid was designed from scratch, we made the input return loss (and therefore also the closely related isolation) one of the primary optimization goals.

III. Design

A brief description of the major waveguide components (the hybrid and the LO coupler), together with the key simulation results, will be given here. An extended discussion of many of the design considerations, as well as the description of the remaining waveguide components, can be found in [1]. All simulations have been carried out with CST Microwave Studio.

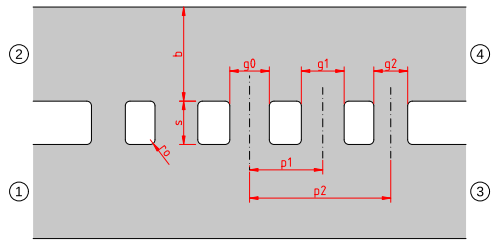

Fig. 3. Layout of the quadrature hybrid. The numbers in circles denote the port numbers as used in the S-parameter plots. Dimensions (in μm): a 400, b 200, s 92, p_1 156, p_2 300, g_0 84, g_1 91, g_2 72, r_o 10.

Overall, a 400×200 μm waveguide was chosen for reasons presented in Section II-A, as well as compatibility with our existing ALMA Band 9 mixer back pieces.

A. Quadrature Hybrid

The quadrature hybrid (see Fig. 3) is a conventional five-branch coupler, kept straight to avoid parasitic trapped modes [10]. As discussed above, the main optimization goal was the reduction of the input reflection (S_{11}) and the isolation (from here on called S_{21}, identical to S_{43} because of symmetry). The optimization was carried out by iteratively modulating the slot positions and widths.

Fig. 4(a) shows a representative set of simulated S-parameters for the resulting geometry. All other S-parameters can be obtained by permutation of the indices. The gain and phase balance and the total power transmission are shown in Fig. 4(b). The crucial isolation factor ($|S_{21}|^2$) is below -24 dB within the band, considerably lower than in the previous design (which was about -18 dB). At the same time, the gain and phase errors are within ± 0.4 dB and $\pm 0.4°$, respectively. From the (complex) S-parameters, the hybrid's contribution to the IRR can be derived using

$$\mathrm{IRR} = 20 \cdot \log_{10} \frac{|S_{41} - (-i)S_{31}|}{|S_{41} + (-i)S_{31}|}$$

which is the IRR when all other components would be perfect. This is shown as the curve labeled "IRR" in the top panel. The worst-case point in the band is about -33 dB, which gives the upper limit for the overall image rejection possible with this design.

B. LO Coupler

The LO is coupled in with a two-branch directional coupler, shown schematically in Fig. 5, with the simulated S-parameters in Fig. 6. The design was optimized to reduce S_{11} as much as possible to minimize any "ordinary" standing wave between the coupler and the SIS mixer device. The coupling factor is set at a rather low value of -13 dB to minimize insertion loss (about 0.25 dB). With the power provided by modern LO sources, this is still more than adequate to pump the mixers optimally.

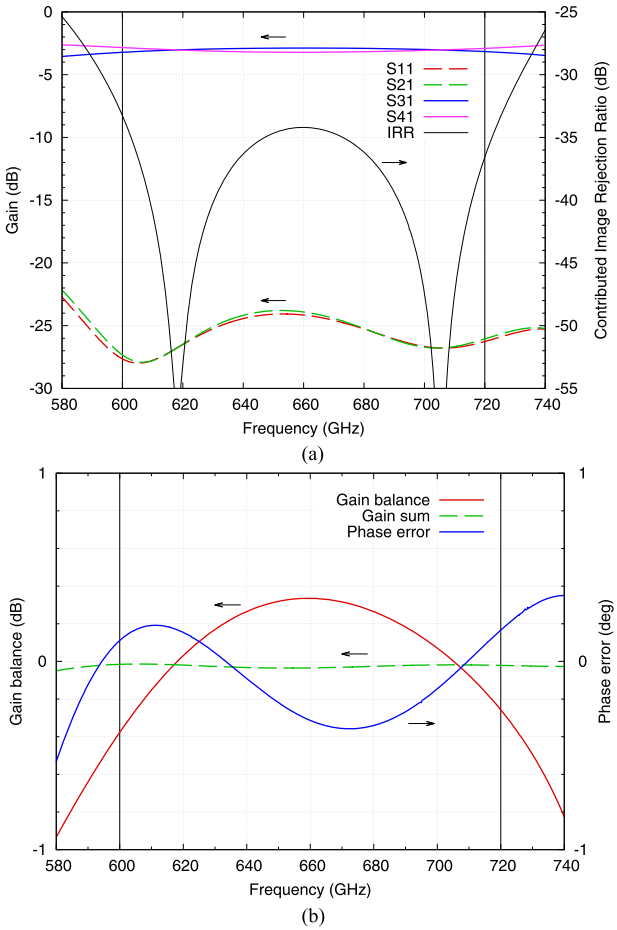

Fig. 4. (a) Simulated S-parameters of the hybrid and the hybrid's contribution to the IRR (black line). (b) Gain balance $|S_{31}|^2/|S_{41}|^2$, phase error $\arg(S_{31}) - \arg(S_{41}) - 90°$, and the total power throughput ("gain sum") $|S_{31}|^2 + |S_{41}|^2$.

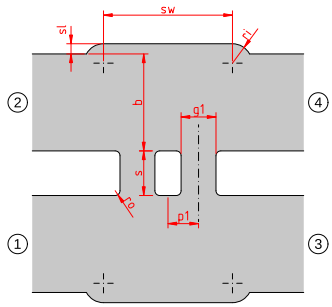

Fig. 5. Layout of the LO coupler. Dimensions (in μm): a 400, b 200, s 92, p_1 63, g_1 72, s_w 266, s_l 21, r_i 40, r_o 10.

IV. Results

After testing a prototype of the block, machined in-house at the Universidad de Chile, four high-quality operational blocks were produced by GARD.[1]

For the baseline reference, these blocks were first tested with exactly the same SIS devices, as well as horns and other auxiliary components, used in the characterization of the previous design [5]. The mixers were tested in a modified copy of a standard ALMA Band 9 receiver cartridge. The noise temperature was determined with a 300/77-K hot–cold Y-factor measurement, the IRR according to the method described in [11].

[1]Group for Advanced Receiver Development, Chalmers University of Technology, Gothenburg, Sweden.

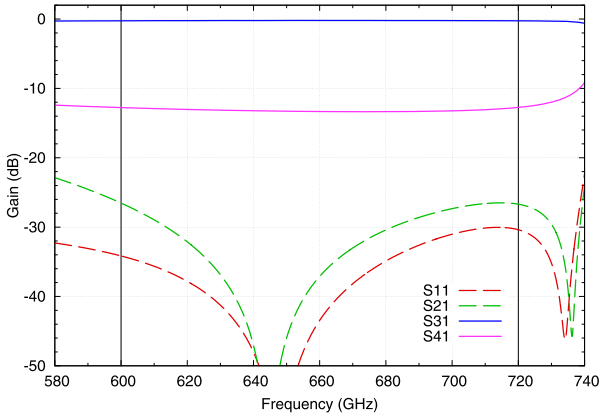

Fig. 6. Representative set of S-parameters of the simulated LO coupler. The coupling $|S_{41}|^2$ is set at -13 dB, while the input reflection $|S_{11}|^2$ and isolation $|S_{21}|^2$ were minimized.

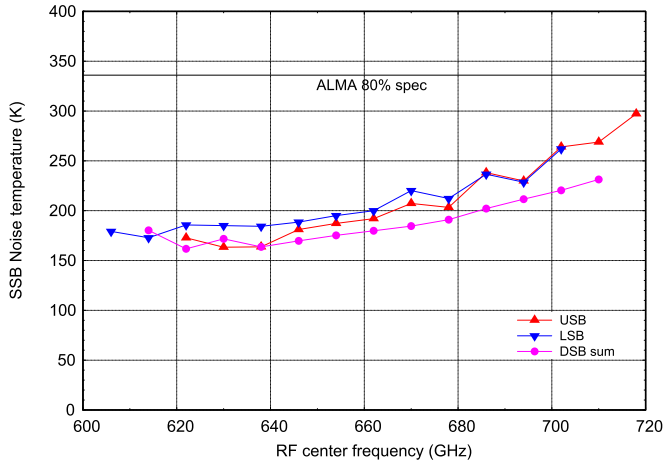

Fig. 7. SSB noise temperature of both upper and lower sidebands as a function of the RF frequency corresponding to the center of the IF band (LO + 8 GHz, LO − 8 GHz for upper sideband (USB) and lower sideband (LSB), respectively). For reference, the sum of the DSB noise temperatures of the two individual SIS mixer devices is plotted as well (average of two measurements). According to the ALMA Band 9 specifications, the SSB noise temperature should be below 336 K (horizontal line) for at least 80% of the band, and below 500 K for the entire band.

A. Noise Temperature

The single-sideband (SSB) noise temperature of the first GARD-produced block, using the same reference pair of SIS devices, is shown in Fig. 7. To give an idea of the noise penalty incurred by the waveguide structures, the sum of the DSB noise temperatures of the individual mixer devices is plotted as well. If all other components were lossless, the SSB noise temperatures should correspond to this sum. In the plot, an excess noise temperature of about 20 K is observable, corresponding to about 0.5-dB loss in the waveguide structure. This value contains

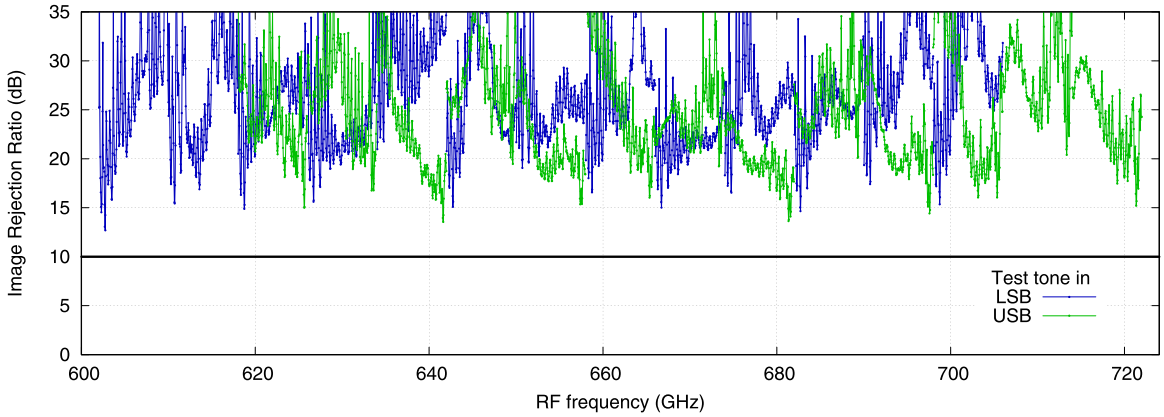

Fig. 8. IRR of the first production hybrid block as a function of RF observation frequency (i.e., the frequency of the test tone used to determine the IRR). The typical specification for 2SB ALMA bands (10-dB minimum) is indicated with a horizontal line.

several uncertainties, however, as the DSB and SSB measurements were performed with different IF isolators, IF amplifiers, and LO multipliers, all of which contribute more or less noise. Overall, we roughly estimate the uncertainty of the excess noise temperature to be ± 10 K. Despite this, it is clear that ALMA-class specifications can be met with margin, provided that SIS junctions of sufficiently high quality are available.

B. Image Rejection

Fig. 8 shows the IRR obtained with the first production block. The IRR is above 15 dB in almost all points, with an ample margin within the typical specification (≥ 10 dB) of current receivers.

This measurement was done in the finished state including the Ti coating ($\approx 0.8\ \mu$m thick) of the distributed loads. Compared to the measurement done just before coating, a slight change in the IRR pattern was observed but no marked overall improvement. After this repeated with the second block, we decided not to apply the coating for the remainder of the blocks, as it is a slightly risky operation. We conclude that (apart from possibly a small contribution from the extra attenuation due to the long waveguides to the loads) the main improvement is due to the mitigation of the unbalanced interference effects mentioned in Section II-B. Comparison with earlier prototypes also reveals that careful and burr-free machining can contribute 5 dB or more to the obtainable IRR, which is easy to understand considering that the image rejection is based on the precise cancellation of large signals, making the system very sensitive to any break in symmetry.

Three out of four production blocks show very similar IRR performance. The fourth has a slightly reduced worst-case IRR (down to about 13 dB using the same mixers), although still quite usable. Probably, this is due to tiny burrs or other remaining imperfections to be investigated and hopefully remedied in a later stage.

C. Mixer Pairing

Apart from the symmetry within the RF and IF hybrids, another important contributor to the image rejection is the matching of the properties of the SIS mixer devices (here called "pairing" to avoid confusion with impedance matching). It turns out that our set of reference mixers, which were chosen rather arbitrarily years ago, actually are exceptionally well paired, and it took some effort to find other pairs among our stock of left-over Band 9 devices that equaled this performance.

The most obvious pairing criterium is, of course, the mixer gain (as a function of frequency). In principle, the mixer gain can be adjusted slightly by changing the bias voltage. However, the Band 9 junctions have very little gain variation over the usable bias tuning range, which is confined by the Josephson peaks on one side and the gap on the other. Only very close to the gap, the gain varies significantly, but only at a high cost in noise temperature and stability. This means that, for this type of junction, static pairing is very important.

We performed a series of measurements with about a dozen differently paired mixers. Most of them were chosen to match gain and normal-state resistance R_N as closely as possible, but some were mismatched on purpose in an attempt to bracket the usable parameter ranges.

Unfortunately, it turned out that there is no simple correlation between the mixer gains as determined in DSB measurements and the obtained IRRs. Fig. 9 shows an overview of the gain ratios of all tested mixer combinations as a function of LO frequency, grouped in three IRR quality classes. Clearly, most of the pairs with the worst performance (red down-pointing triangles) have wildly varying gain ratios, as expected. However, the ones with the flattest ratios close to 0 dB are not the best performers; they tend to occupy the middle range (blue circles). Several of the best ones (green up-pointing triangles) tend to show much more variation. Obviously, other parameters play significant roles as well.

Other comparisons with, e.g., normal-state resistance R_N, noise temperature T_n, and pumping current show some tentative correlations, but none on its own seems a good predictor for the image rejection.

One interesting observation is that the better IRRs are obtained with junctions that, during production, were close together on the same wafer (and furthermore, none of the pairs from different wafers performed very well). Since it is known

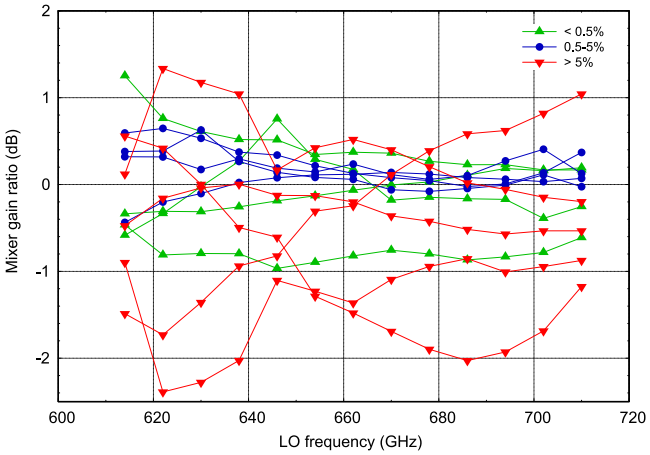

Fig. 9. Overview of the gain ratios of all tested SIS mixer pairs (in the same hybrid block) as a function of LO frequency. The curves have been grouped in three IRR categories: very good ones with less than 0.5% of the IRR data points below 15 dB, reasonably good ones with up to 5% points below 15 dB, and less good ones with more than 5% below 15 dB. Notably, the best ones are not the ones closest to 0 dB.

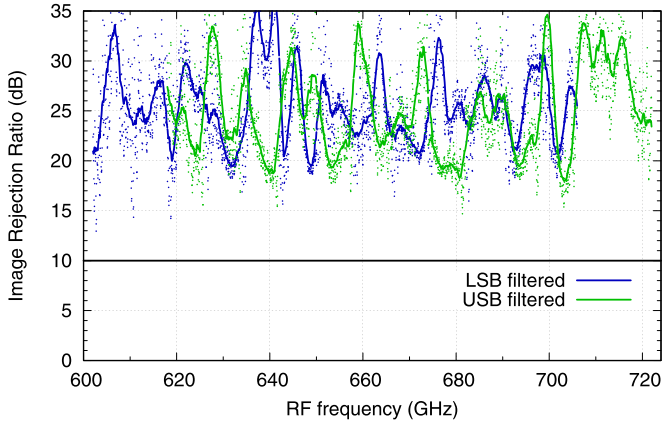

Fig. 10. IRR (not the same mixer pair as in Fig. 8) filtered with a 2-GHz-wide sliding window, in order to separate the RF-induced effects from the IF-induced ones. The dots represent the unfiltered data. Note that the filter is simply applied in the dB domain, not on the linear ratios; this is debatable, but for the ratios of interest (i.e., the lowest ones), this makes no large qualitative or quantitative difference.

that there are thickness gradients in the SiO_2 dielectric layers over the wafer (and certainly between wafers), this makes us speculate that it is actually the phase characteristics of the on-device tuning structures that could account for the unpredictable IRR performance. At the moment, we do not have simple means to measure the phase transfer of a single mixer.

For the current set of four 2SB mixers intended for near-future deployment, the simple brute-force testing campaign that we performed was adequate to find the required number of mixer pairs. For any future large-scale project, a better understanding of the underlying mechanisms would be very beneficial.

Finally, it should be noted that although many mixer pairs show unsatisfactory results when compared to the best ones, all but one of them still delivered more than 10 dB of IRR over the entire band.

D. Influence of the IF System

When image rejection curves such as in Fig. 8 are studied in detail, it is clear that apart from the obvious large-scale (order 10 GHz) patterns resulting from residual imbalances in the RF circuit, there are persistent small-scale (subgigahertz) ripples. Because of their length scale, and their behavior when components are replaced, we attribute these to the IF system. To get an idea of the possible obtainable IRR with the current waveguide structure, provided that the IF system is improved significantly, Fig. 10 shows the IRR filtered with a 2-GHz-wide sliding window, removing most of the fast (IF-related) ripples. In this particular case, the 18-dB IRR should be obtainable over the entire band.

In current receivers, IF ripples, which are mainly caused by standing waves due to bad impedance matching of mixers and low-noise amplifiers (LNAs), are usually suppressed by inserting isolators (a.k.a. circulators) between the mixers and the LNAs. For 4–8-GHz four-channel or 4–12-GHz two-channel systems such as the classical ALMA receivers, this is still feasible. The primary purpose of the 2SB mixers in the current study, however, namely deployment in four-channel ALMA-class receivers and small focal-plane arrays with IF bands of at least 4–12 GHz, calls for a more compact system integration. The bulky, expensive, and lossy 4–12-GHz isolators become the bottleneck both for performance and for miniaturization.

The IF system of the baseline receiver, with which all results presented above were obtained, consisted of a 4–12-GHz cryogenic quadrature hybrid [12], followed by two isolators and two LNAs, all connected by short coaxial cables.

We performed a simple experiment, where we removed the isolators from the IF chain. The standard Band 9 LNAs [13] (with an input reflection of about −4 dB) were replaced by two 4–12-GHz monolithic microwave-integrated circuit amplifiers provided by CAY[2] (similar to the ones described in [14]) as contribution to the RadioNet3 AETHER workpackage.[3] These amplifiers have an improved input reflection (around −10 dB, worst in-band point −7 dB). Another essential feature in this context is their integrated bias-tee, which we need because, up to now, we supplied the mixer bias through the load ports of the isolators.

The resulting image rejection is shown in Fig. 11. Because of the strongly increased ripple due to reflections in the IF system, the worst-case IRR is reduced by about 5 dB, making it touch the typical 10-dB specification. On the other hand, by eliminating the loss in the isolators, the noise temperature curves (not shown) go down by about 10 K, without significantly changing their shape.

Surprisingly, when the IF passbands of the two configurations are compared, as done in Fig. 12, no significant increase in ripple amplitude is seen. Apparently, the observed deterioration of the IRR is not simply due to standing waves. A detailed model of the mechanisms that explain the influence of standing waves and other reflections in the IF system is yet to be constructed. It is

[2]Centro Astronómico de Yebes, Spain.
[3]FP7 Grant Agreement no. 283393.

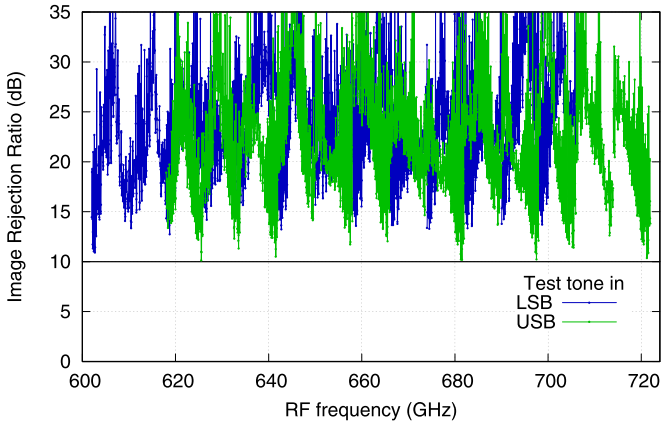

Fig. 11. IRR with the same 2SB mixer block and SIS devices as in Fig. 8, but with the isolators removed and the LNAs replaced by types with improved input reflection.

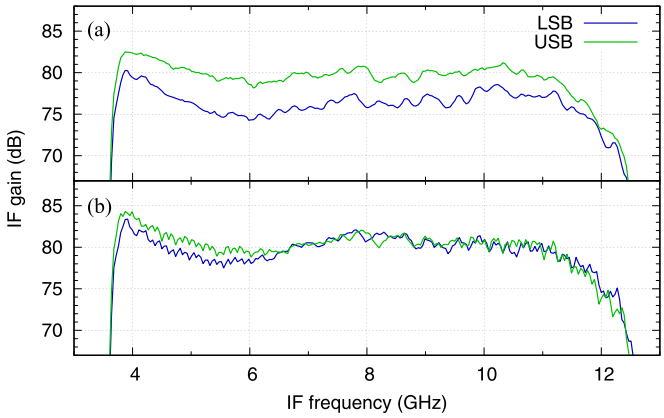

Fig. 12. IF gains from the mixers to the output of the receiver, measured by biasing both mixers above the gap at two voltages to use them as shot-noise generators. (a) With IF isolators and tradition LNAs. (b) Without isolators but with improved-input-match LNAs.

likely, however, that effects similar to the unbalanced reflection found in the RF path are responsible, rather than simple standing waves. One complicating factor here is that both sides of the signal path (i.e., the SIS devices and the LNAs) are reflective to a considerable degree. In the RF path, at least one side (consisting of the RF feedhorn and RF load) presents a good impedance match. We intend to construct a full IF model in the near future.

V. Conclusion

We designed, built, and tested a new 2SB mixer assembly for the 600–720-GHz band (ALMA Band 9). By concentrating on the input matching and isolation of the quadrature hybrid and associated waveguide components, rather than on the phase and amplitude balance, we minimized standing waves and especially asymmetric reflection paths, which are highly detrimental to the IRR. IRRs in excess of 15 dB are obtained repeatably with different blocks and mixer pairs. At the same time, the SSB noise temperature is increased by not more than 20–30 K with respect to the bare mixer devices, corresponding to a loss of about 0.5 dB in the waveguide structure.

When the contributions of reflections in the IF system are filtered out, the worst-case image rejection can be as high as 18 dB with well-matched mixers. This still includes the normal phase and amplitude imperfections of the IF hybrid, however, and so is expected to be a good indication of what can be achieved with highly matched IF amplifiers. In less demanding cases, the ample margin in the IRR on the RF side can be used to build a system with reasonably matched amplifiers that still meets a typical 10-dB IRR specification.

Acknowledgment

The authors would like to acknowledge M. Bekema and R. de Haan Stijkel (Kapteyn Astronomical Institute) for their help in integrating and measuring the mixer assembly, and A. Kaverzin, J. G. Holstein, J. Liu, and H. Martijn de Roosz (Physics of Nanodevices, University of Groningen) for support with the Ti deposition. The envelope of the modular mixer block and the associated components were originally designed by G. Gerlofsma. The authors would like to recognize the efforts of the group led by T. M. Klapwijk (Delft University of Technology) in producing the mixer devices during the ALMA Band 9 production. Finally, the authors thank J. Adema and A. Koops for their organizational and management support.

References

[1] R. Hesper, A. Khudchenko, A. M. Baryshev, J. Barkhof, and F. P. Mena, "A new high-performance sideband-separating mixer for 650 GHz," *Proc. SPIE*, vol. 9914, 2016, Art. no. 99140G. [Online]. Available: http://dx.doi.org/10.1117/12.2233065

[2] A. Khudchenko *et al.*, "First results of the sideband-separating mixer for ALMA band 9 upgrade," in *Proc. 22nd Int. Symp. Space Terahertz Technol.*, Charlottesville, VA, USA, 2011, pp. 143–149.

[3] A. Khudchenko *et al.*, "Sideband separating mixer for 600–720 GHz for ALMA band 9 upgrade," *Proc. SPIE*, vol. 8452, Sep. 2012, Art. no. 845214.

[4] F. Mena *et al.*, "Design and performance of a 600–720-GHz sideband-separating receiver using AlO_x and AlN SIS junctions," *IEEE Trans. Microw. Theory Techn.*, vol. 59, no. 1, pp. 166–177, Jan. 2011.

[5] R. Hesper, G. Gerlofsma, F. P. Mena, M. C. Spaans, and A. M. Baryshev, "A sideband-separating mixer upgrade for ALMA band 9," in *Proc. 20th Int. Symp. Space Terahertz Technol.*, Charlottesville, VA, USA, Apr. 2009, pp. 257–260.

[6] A. M. Baryshev *et al.*, "The ALMA band 9 receiver—Design, construction, characterization, and first light," *Astron. Astrophys.*, vol. 577, May 2015, Art. no. A129.

[7] A. Khudchenko, R. Hesper, A. M. Baryshev, J. Barkhof, and F. P. Mena, "Modular 2SB SIS receiver for 600–720 GHz: Performance and characterization methods," *IEEE Trans. THz Sci. Technol.*, vol. 7, no. 1, pp. 2–9, Jan. 2017.

[8] A. Pippard, "The surface impedance of superconductors and normal metals at high frequencies. II. The anomalous skin effect in normal metals," *Proc. Roy. Soc. A, Math., Phys., Eng. Sci.*, vol. 191, pp. 385–399, 1947.

[9] G. E. H. Reuter and E. H. Sondheimer, "The theory of the anomalous skin effect in metals," *Proc. Roy. Soc. A, Math., Phys., Eng. Sci.*, vol. 195, pp. 336–364, 1948.

[10] A. Morgan and S.-K. Pan, "Graphical prediction of trapped mode resonances in sub-mm and THz networks," in *Proc. 23rd Int. Symp. Space Terahertz Technol.*, Charlottesville, VA, USA, 2012, pp. 39–42. [Online]. Available: http://search.space-thz.org/catalog/2012039042

[11] A. R. Kerr, S.-K. Pan, and J. E. Effland, "Sideband calibration of millimeter-wave receivers," in *ALMA Memo Series*, Memo 357, Mar. 2001. [Online]. Available: http://library.nrao.edu/alma.shtml

[12] I. Malo-Gómez, J. D. Gallego-Puyol, C. Diez-González, I. López-Fernández, and C. Briso-Rodríguez, "Cryogenic hybrid coupler for ultra-low-noise radio astronomy balanced amplifiers," *IEEE Trans. Microw. Theory Techn.*, vol. 57, no. 12, pp. 3239–3245, Dec. 2009.

[13] I. López-Fernández, J. D. Gallego Puyol, C. D. González, and A. B. Cancio, "Development of cryogenic IF low-noise 4-12 GHz amplifiers for ALMA radio astronomy receivers," in *IEEE MTT-S Int. Microw. Symp. Dig.*, Jun. 2006, pp. 1907–1910.
[14] B. Aja Abelan *et al.*, "4–12- and 25–34-GHz cryogenic mHEMT MMIC low-noise amplifiers," *IEEE Trans. Microw. Theory Techn.*, vol. 60, no. 12, pp. 4080–4088, Dec. 2012.

Ronald Hesper received the M.Sc. degree in experimental solid-state physics from the University of Leiden, Leiden, The Netherlands, and the Ph.D. degree in experimental solid-state physics from the University of Groningen, Groningen, The Netherlands.

Since 2000, he has been an Instrument Scientist with the Kapteyn Astronomical Institute, University of Groningen. From 2000 to 2008, he was involved in the technological development of the ALMA Band 9 receivers, including the process of industrialization, as well as related projects like the CHAMP+ mixer arrays for APEX, from 2008 to 2013, on the development of a sideband-separating mixer upgrade for the ALMA Band 9 receivers, and, from 2013 to the beginning of 2015, on the industrialization of the ALMA Band 5 receivers. He is also involved in the development of new (arrayable) heterodyne detector technologies at frequencies around 1 THz.

Andrey Khudchenko received the M.S. degree in applied physics and mathematics and Ph.D. degree in radiophysics from the Moscow Institute of Physics and Technology, Moscow, Russia, in 2007 and 2009, respectively.

From 2004 to 2008, he was an Engineer and, in 2009, a Researcher with the Kotel'nikov Institute of Radio Engineering and Electronics, Russian Academy of Sciences, Moscow. From 2009 to 2016, he was an Instrument Scientist with the Netherlands Institute for Space Research, Groningen, The Netherlands. Since 2016, he is with the Kapteyn Astronomical Institute, University of Groningen, where he is involved with the development of new heterodyne terahertz instruments. It includes the development of sideband-separating receiver for the ALMA band 9, CHAMP+ high mixers for the APEX telescope, and work on stabilization of quantum cascade lasers for hot electron bolometer receivers.

Andrey M. Baryshev received the master's degree (*summa cum laude*) in physical quantum electronics from the Moscow Institute of Physics and Technology, Moscow, Russia, in 1993, and the Ph.D. degree from the Technical University of Delft, Delft, The Netherlands, in 2005.

He is currently a Senior Instrument Scientist. Since 1998, he has been with the SRON Low Energy Astrophysics Division and the Kapteyn Astronomical Institute, University of Groningen, Groningen, The Netherlands. Since 2000, he has been involved in a joint effort to develop the SIS receiver (600–720 GHz) for ALMA. In 2013, he became an Associate Professor of astronomical instrumentation for the far-infrared with the Kapteyn Astronomical Institute, University of Groningen. His main research interests include the areas of heterodyne and direct detectors for large focal plane arrays at terahertz frequencies and quasi-optical system design and experimental verification.

Dr. Baryshev was the recipient of a Netherlands Organisation for Scientific Research-VENI grant for research on heterodyne focal plane array technology in 2008, and an EU Commission Starting Researcher Grant for work on direct detector focal plane arrays in 2009.

Jan Barkhof received the M.Sc. degree in applied physics from the University of Groningen, Groningen, The Netherlands.

From 1999 to 2004, he was an Optical Researcher with Pfizer, where he was involved with an accommodating intraocular lens. Since 2004, he has been a Test Engineer with the Kapteyn Astronomical Institute, University of Groningen, developing test systems and software for verifying the quality of ALMA Band 9 and Band 5 receivers.

Fausto Patricio Mena received the B.S. degree in physics from the Escuela Politécnica Nacional, Quito, Ecuador, in 1994, and the M.S. and Ph.D. degrees in physics from the University of Groningen, Groningen, The Netherlands, in 2000 and 2004, respectively.

In 2004, he joined the Low Energy Division, Netherlands Institute for Space Research, as an Instrument Scientist. Since 2008, he has been a Professor with the Department of Electrical Engineering, Universidad de Chile, Santiago, Chile, where he leads the Millimeter and Submillimeter Wave Laboratory.